THE JOURNAL OF PHYSICAL CHEMISTRY Letters

Physical Insights into Light Interacting with Matter

Directional Light Emission from Layered Metal Halide Perovskite Crystals

Grant W. Walters, Louis Haeberle, Rafael Quintero-Bermudez,
Julien Brodeur, Stéphane Kéna-Cohen, and Edward H. Sargent

J. Phys. Chem. Lett., **Just Accepted Manuscript** • DOI: 10.1021/acs.jpclett.0c00901 • Publication Date (Web): 15 Apr 2020

Directional Light Emission from Layered Metal Halide Perovskite Crystals

*Grant Walters[†§], Louis Haeberlé[‡§], Rafael Quintero-Bermudez[†], Julien Brodeur[‡], Stéphane Kéna-Cohen[‡], Edward H. Sargent[†]**

[†]Department of Electrical and Computer Engineering, University of Toronto, 35 St. George Street, Toronto, Ontario, M5S 1A4 Canada

[‡]Department of Engineering Physics, Polytechnique Montréal, Montréal, Québec, H3C 3A7, Canada

Corresponding Author

*Email: ted.sargent@utoronto.ca

Metal halide perovskites are being increasingly explored for use in light emitting diodes (LEDs), with achievements in efficiency and brightness charted across the spectrum. One path to further boosting the fraction of useful photons generated by injected electrical charges will be to tailor the emission patterns of devices. Here we investigate directional

emission from layered metal halide perovskites. We quantify the proportion of in-plane versus out-of-plane transition dipole components for a suite of layered perovskites. We find that certain perovskite single crystals have highly anisotropic emissions and up to 90% of their transition dipole in-plane. For thin films, emission anisotropy increases as the nominal layer thickness decreases and is generally greater with butylammonium cations than with phenethylammonium cations. Numerical simulations reveal that anisotropic emission from layered perovskites in thin film LEDs may lead to external quantum efficiencies of 45%—an absolute gain of 13% over equivalent films with isotropic emitters.

TOC GRAPHICS

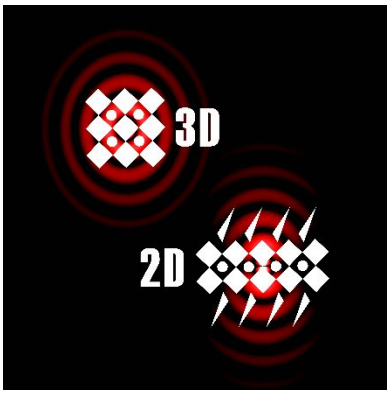

KEYWORDS transition dipole moment, photoluminescence, quantum well, solution processed, out-coupling

Metal halide perovskites are capable of highly efficient emission at wavelengths spanning the visible light spectrum. Their impressive photoluminescence quantum yields, along with their electronic attributes as semiconductors and their solution processing, have led to successes as the active materials in inexpensive thin film light emitting-diodes (LEDs). These devices have been able to achieve impressive external quantum efficiencies (EQE) and brightness at red (21% EQE[1], 2000 cd•m^{-2} brightness[2]), green (20% EQE[3], 91000 cd•m^{-2} brightness[4]), and blue (9.5% EQE[5], 4000 cd•m^{-2} brightness[6]) emission wavelengths. These accomplishments have propelled metal halide perovskites as candidates for use in new display and lighting technologies.

While advances in materials quality and composition offer possible further improvements to LED performance, device design enhancements have the potential to also boost performance. One major optical loss in current thin film devices is the photons that become trapped through waveguiding and total internal reflection. A strategy to

overcome this is to employ an active material with an anisotropic emission pattern, preferentially directed normal to the thin film stack and thereby leading to a greater fraction of useful photons generated. This approach has been leveraged and studied for organic LEDs[7–9] and inorganic nanocrystals[10,11] but remains largely untouched for perovskite LEDs. Only a few recent works have broached the topics of out-coupling and orientational emission from a select few perovskite materials.[12–17] Researchers have shown that thin films of perovskite nanocrystals can be engineered to improve light extraction[12,16], studied optical anisotropy in purely 2D perovskites[13], and examined out-coupling from LEDs with bulk perovskite films[15,17].

Different morphological variations of metal halide perovskites have shown success as LED materials: bulk-like crystallites,[3,4] nanocrystals and nanoplatelets,[1,18] and layered structures.[6,19,20] Layered perovskites, in particular, can possess exceptionally high exciton binding energies and radiative recombination rates.[21–23] This is due to strong quantum and dielectric confinement effects that arise from the disruption of the normally periodic perovskite lattice with bisecting organic layers. These organic layers typically consist of ammonium terminated alkyl or aryl molecules that bind to and terminate the

perovskite lattice. Perovskite quantum wells with widths defined by the number of perovskite octahedral units (*n*) can be synthesized. These layered perovskites, although fundamentally anisotropic in nature, can be highly disordered when synthesized as thin films[19,24,25] for use in LEDs.

Here, we investigate the orientational emission patterns of a broad range of layered metal halide perovskite systems with the aim of revealing opportunities for directed emission and improved emission efficiency from LEDs. We use single crystals of layered perovskite to understand the ultimate potential of these materials for directed emission and find that they can have 90% of their transition dipole moment in the plane of the quantum wells. This preferential alignment of the excitonic state then translates to a large portion of the emission being oriented about the normal direction. As contrast to the ideality of single crystals, we report similar measurements for a spectrum of layered perovskite thin film materials that have optoelectronic relevance. Their emission patterns vary but can still be substantially orientational with around 80% of their transition dipole moment in the plane of the film. In general, because of disorder and funneling, the films exhibit more isotropic emissions than the crystals. This illustrates that further advances

in LED efficiency can be made by engineering perovskite films that have an ordered structure akin to that of single crystals. We complement our measurements with an analysis of the improvements to be made to device efficiency and find that EQE's of 45% are possible with entirely oriented layered perovskites.

The directional emission patterns for single crystals were measured using a Fourier-space microscopy setup, which measures photoluminescence (PL) as a function of the in-plane momentum, *k*. Single crystal flakes of layered methylammonium lead iodide perovskites with butylammonium ligands ($BTA_2MA_{n-1}Pb_nI_{3n+1}$, n = 1, 2, 3) were synthesized according to a reported slow-cooling precipitation method[26], exfoliated onto substrates, and probed with the microscopy setup. Panels a) and b) in Figure 1 show the intensity of p- and s-polarized emission, respectively, as a function of the in-plane wavevector for an n = 3 crystal. We also provide the corresponding emission spectrum and a photograph of the crystal in panel c). The PL spectrum shows a single well-defined peak at 650 nm (PL peaks for all materials provided in Table S1), illustrating the n = 3 phase and crystal purity.

The k-space intensity profiles were fit to the result obtained from a dyadic Green's function calculation[27,28], which accounts for anisotropy in the dipole orientation and in the refractive index of the perovskite layer. This allows us to determine the fraction of the transition-dipoles that align along the plane of the crystal flakes—and so too the plane of the quantum wells. This fraction, α, is plotted in Figure 1d for the different n values. A purely isotropic emitter would have an α value of about 0.66 as two thirds of its emissions will match to the plane of the two-dimensional material, while a purely anisotropic emitter with its transition dipole oriented within the plane of the two-dimensional material would have an α value of unity. All three crystals yielded α values near 0.9, indicating strongly anisotropic emissions. The layer-upon-layer ordering within the single crystals then suggests that the transition dipole moments of excitons bound within the perovskite quantum wells are similarly anisotropic. The α values for the three materials do show a slight increase with increasing n; however, we note that the data points overlap with the neighbouring confidence intervals, and so we do not purport any trends across well widths. Given that the bulk material should have an isotropic distribution, the α values

should decrease as *n* increases. As the layered perovskites have quantum wells that are only a few atomic units wide, this trend may not be resolvable until higher *n* values.

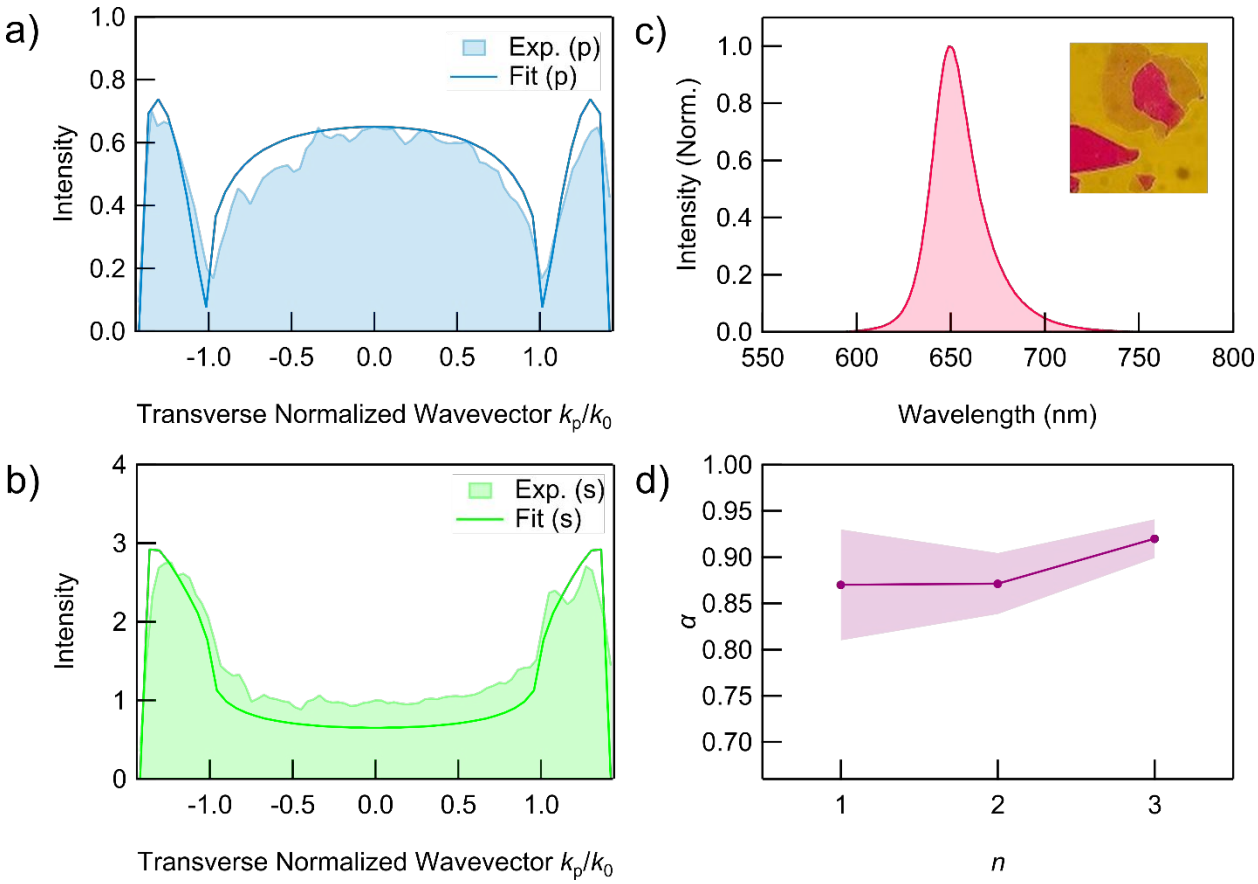

Figure 1. Directional emission from layered perovskite single crystals. a) and b) PL intensity as a function of k-space wavevector for p- and s-polarized emission respectively. Data was obtained from an *n* = 3 $BTA_2MA_2Pb_3I_{10}$ single crystal flake with a PL emission spectrum provided in c). Inset shows the single crystal flake. Fitting indicated that 95% of the transition dipole was in-plane. d) Fraction of in-plane transition

dipoles for butylammonium/methylammonium lead iodide layered perovskite single crystals. Vertical shading indicates the 95% confidence interval.

In addition to the single crystal experiments, we studied the directional emission patterns of layered perovskite thin films on glass substrates. In this case, thin films were mounted to a hemisphere with index matching fluid and the angle-resolved PL was directly measured. We varied the film compositions across three parameters: ligand (butylammonium, BTA; phenethylammonium PEA, hexylammonium, HXA), organic cation (methylammonium, MA; formamidinium, FA), and well width. Three series of compositions were measured: $BTA_2MA_{n-1}Pb_nI_{3n+1}$, $PEA_2MA_{n-1}Pb_nI_{3n+1}$, and $BTA_2FA_{n-1}Pb_nI_{3n+1}$. For these series, we denote the well width as $\langle n \rangle$, reflecting that these are nominal values and that a distribution of layer widths exists in the films.[19,24] The films in these $\langle n \rangle$ series were fabricated using the spin-casting method with antisolvent quenching.[19] We also measured two other films at the extremes of the $\langle n \rangle$ film series. The first was a film comprised of $n = 1$ nanoplatelets having a composition of hexylammonium lead iodide. The nanoplatelets were synthesized using a drop-wise precipitation method

and deposited onto substrates centrifugally.[29,30] The second film was the bulk perovskite archetype—methylammonium lead iodide ($n = \infty$). Panel a) in Figure 2 shows a sample dataset for a film of $\langle n \rangle = 3$ methylammonium lead iodide perovskite with butylammonium ligands. The solid lines in this figure are fits to the optical dipole emission model.[27,28] This allows us to determine the α parameter for each film; the values are plotted in panel b) of Figure 2. In the case of thin films, α does not necessarily indicate the fraction of the transition dipole moment that is in the plane of the quantum wells as disorder within the films may randomize the orientations of the quantum wells themselves.

Several trends are clear amongst the thin film samples. Both films with BTA ligands exhibit α values around 0.8 for the studied $\langle n \rangle$ series. In contrast, the films with PEA show a sudden transition from anisotropic to isotropic emission immediately as methylammonium is incorporated into the films. The remaining two films at the *n* extremes, the nanoplatelet and bulk films, have correspondingly extreme α values: the $n = 1$ nanoplatelet film exhibits highly anisotropic emission, while the bulk film shows nearly isotropic emission (within one standard deviation).

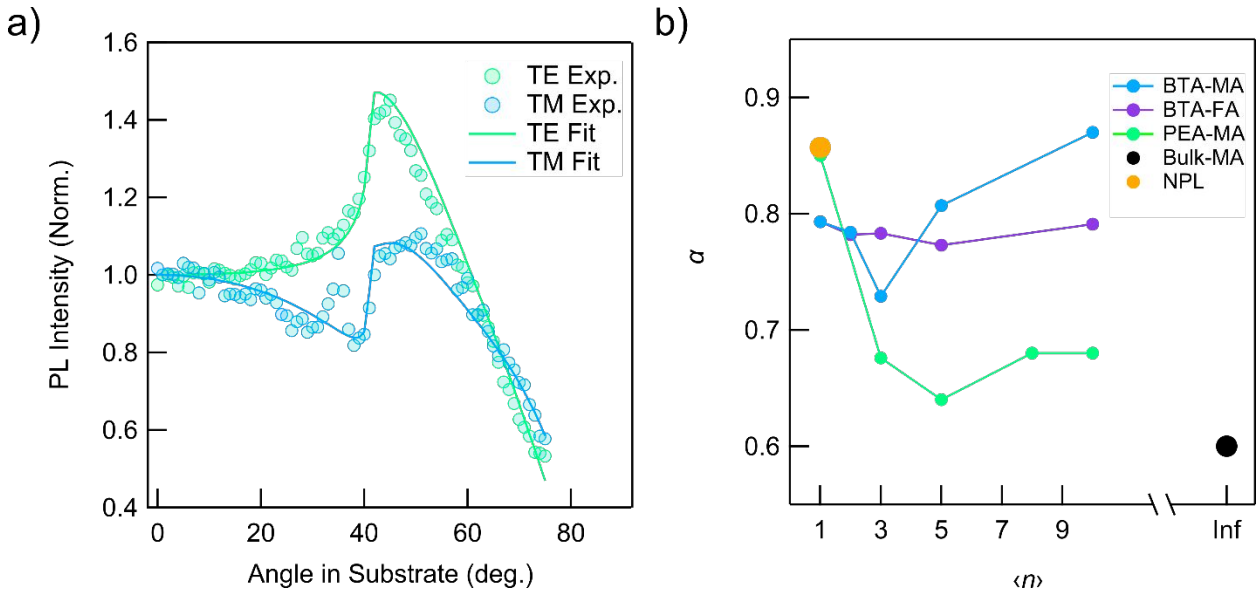

Figure 2. Emission pattern from thin films. a) PL emission intensity as a function of angle in substrate for a $BTA_2MA_2Pb_3I_{10}$ $\langle n \rangle = 3$ thin film on glass. The fraction of in-plane dipoles was determined to be 0.74. b) Fraction of in-plane dipoles for thin film samples with different compositions. The largest standard deviation for any of these measurements was ±0.07.

A combination of material differences amongst the perovskite materials causes the differences in observed α values. Key factors include the quantum well width, well-to-well disorder, heterogeneity of wells, and electronic transfer.

Large fractions of in-plane dipole moment for layered perovskites derive from their two-dimensional structure. The organic barrier ligands confine the excitonic

wavefunctions to the lead halide octahedra, such that they primarily exist over only a few atomic units in the normal direction. In contrast, within the plane of the lead halide layers, the wavefunctions remain delocalized periodic functions. We provide illustrations of the highest occupied and lowest unoccupied molecular orbital wavefunctions calculated using density functional theory (DFT) in Figure 3a that show this. The exciton, represented as the RMS expectation value of the separation between these hole and electron states, follows an oblate shape. While this representation is not truly characteristic of the transition dipole moment for the exciton, it illustrates the anisotropic nature. Moreover, prior computational work has analyzed the symmetries of the band edge wavefunctions in two-dimensional metal halide perovskites and predicted that the fundamental transition exhibits transverse electric (TE) character.[31,32] Thus, optical activity would be restricted to light with an electrical polarization parallel to the perovskite layers. As n increases towards the bulk $n = \infty$ case, the transition dipole moment should tend towards an isotropic distribution. The extrema of the film studies support these ideas, but the intermediate films exhibit dissimilar trends that depend on film composition.

Prior experimental work[24,33] has revealed key differences between spin-casted films with PEA and BTA ligands. Transient absorption spectroscopy has revealed disparateness in the distributions of quantum wells. By fitting the ultrafast bleach features corresponding to the individual wells, the distributions have been elucidated. Films with BTA ligands tend to show considerably greater proportions of low-*n* wells than films with PEA ligands. Grazing incidence wide-angle x-ray scattering measurements has corroborated this finding as well as revealed a preferential tendency of low-*n* wells to align parallel to the substrate and high-n wells to align perpendicular to the substrate. These findings, and the widely reported notion of carrier transfer from between wells, support a picture of more isotropic emission from PEA films than from BTA films, which is what we observe in measured α values.

The anisotropic nature of the excitons can ultimately translate to spatial variations in the power radiated during emission. In Figure 3b, we provide the power radiated per solid angle as a function of angular position for $BTA_2MA_2Pb_3I_{10}$ $\langle n \rangle = 3$ thin films and *n* = 3 single crystals, as calculated using the experimentally determined fractions of in-plane and out-of-plane dipole moments. The only mildly anisotropic dipole distribution for the

thin film samples has an emission pattern that then is similarly only mildly anisotropic, with slight differences in power radiated along different directions. The power radiated in in the directions normal to the films can be evaluated by considering the integrated power radiated into a pair of cones centered about the normal axes. For cones with half-angles of 25 degrees—conservative representations of the optical escape cones for a film on glass, only 32% of the total radiated power from an $\langle n \rangle = 3$ thin film is emitted within the cones. Alternatively, the single crystal sample's large fraction of in-plane dipole moments results in an emission pattern directed primarily normal to the planes of the layered structure; in this case 45% of the total radiated power is directed in these cones.

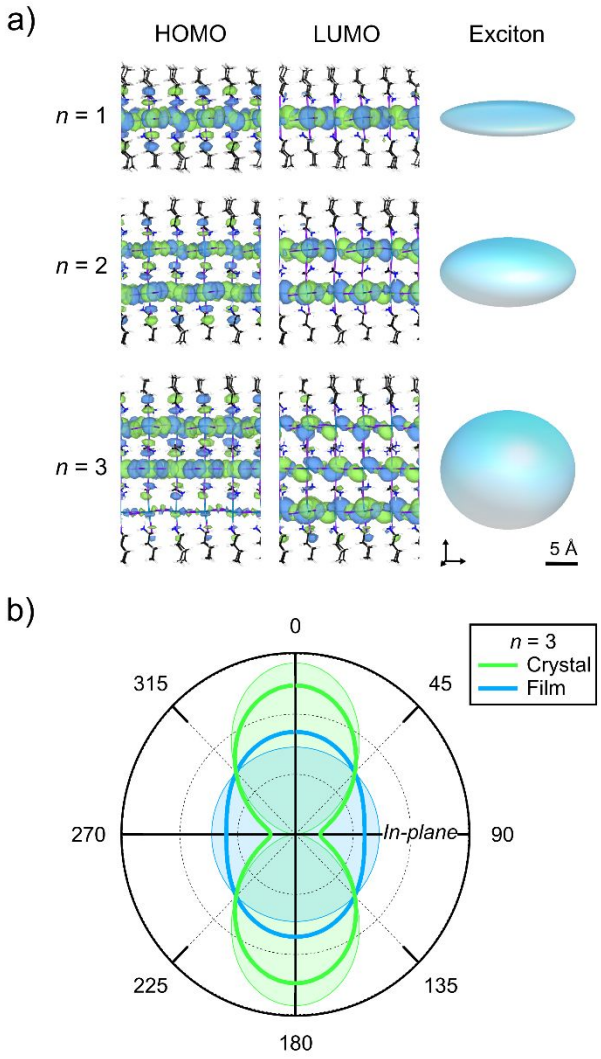

Figure 3. Layered perovskites anisotropic emission. a) DFT calculated highest occupied and lowest unoccupied molecular orbitals for layered perovskites showing localization of the wavefunctions to the lead iodide quantum wells. The excitons, calculated as the RMS expectation value of the separation between electron and hole states, exhibit highly anisotropic shapes. b) Angular power radiation pattern for anisotropic dipole distributions found from the experimentally determined fractions of in-plane and out-of-plane dipole components for $BTA_2MA_2Pb_3I_{10}$ $\langle n \rangle = 3$ thin films and n = 3 single crystals. Shaded areas

display the radiation patterns for a purely in-plane anisotropic dipole distribution and an isotropic distribution. The total power radiated has been normalized for each curve.

The use of anisotropic emitters is a well-accepted strategy for boosting the out-coupling and overall efficiency of thin film LEDs. The anisotropic structure and directed emission of some of the layered perovskites that we have studied, particularly the single crystalline forms, suggests that these perovskites may be capable of device efficiencies unusual amongst thin film materials.

To illustrate the effect of directional emission on LED efficiency, we have calculated the out-coupling efficiencies, and therefore maximum external quantum efficiencies, for a typical LED structure employing layered perovskites (Figure 4a). Numerical finite differences time-domain calculations were done for devices with n = 1, 2, and 3 layered perovskites having either purely isotropic or anisotropic in-plane dipole emitters. The efficiencies (Figure 4b) increase by nearly 50% in going from an isotropic to anisotropic emission. This increase in out-coupling arises from a reduction in surface plasmon modes at the cathode interface, which are only excited by transverse magnetic

(TM) polarizations, and in emission into waveguided modes; prior computational work has quantified these sources of loss in a typical metal halide perovskite LED.[15] Our calculations show that maximum device efficiencies of 20–30% are possible for the isotropic cases, but with anisotropic emission these numbers increase to nearly 30–50%. The device efficiencies also increase from n = 1 to n = 3, which we mainly attribute to decreased reabsorption within the perovskite layer. We also conducted calculations for the bulk n = ∞, with fully isotropic emission, and found an efficiency of 38%, which is slightly greater than the n = 3 case with isotropic emission. We note that the efficiencies reported in Figure 4 are for the extreme dipole distribution cases, and so provide upper limits to efficiency. For the n = 3 case, using the experimentally found dipole distribution for a single crystal, the efficiency limit is slightly lower at 45%.

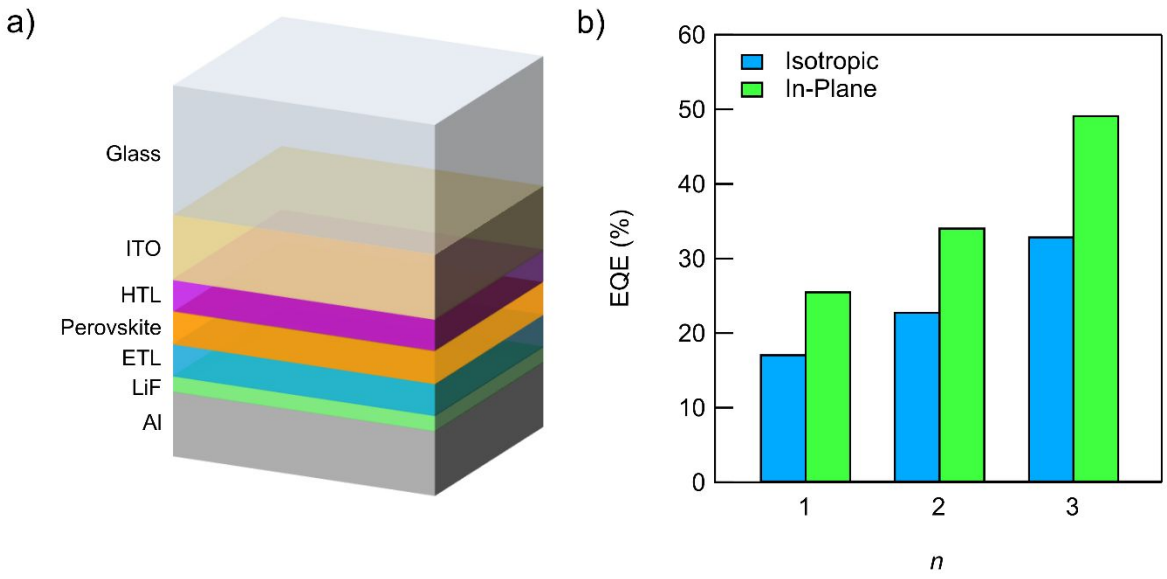

Figure 4. Benefits of anisotropic emission for LEDs. a) Thin-film layer stack representing a typical perovskite LED, which was used in FDTD optical simulations. b) Simulated external quantum efficiency (EQE) for LED structures with iodide layered perovskite emitters having purely in-plane or isotropic transition dipole moment distributions. Unity photoluminescence quantum yield has been assumed and electrical losses have been excluded.

In summary, the two-dimensional constitution of layered metal halide perovskites causes large fractions of the transition dipole moment to reside within the plane of the perovskite layers. This translates to highly anisotropic light emission. Exploiting

directional emission may improve the optical efficiency of LEDs employing these perovskites. Strategies to improve the ordering of the quantum wells within thin films may strengthen the out-coupling of these devices. However, ordering of the quantum wells will lead to carrier transport that is working against the well barriers, and therefore a balance between electrical and optical benefits may be needed. Furthermore, materials engineering to maximize emission anisotropy needs to be carefully checked against changes in photoluminescence quantum yield. Ordering of the quantum wells may affect the effectiveness of strategies used to reduce or circumvent non-radiative recombination pathways in the films. Our findings also indicate a need to account for emission anisotropy in photoluminescence quantum yield investigations of layered perovskites. As anisotropy affects the out-coupling of light from solid materials, it can influence the amount of light reabsorbed and therefore the accuracy of a quantum yield measurement. Methods that rely on quantifying the radiative and non-radiative rates of recombination offer a complementary route to the light emitted over light absorbed approach. Future work in studying emission anisotropy should explore film deposition parameters and other compositional parameters such as the halide content. Advances in crystal growth will also

enable measurements of perovskites with n > 3 and further clarify the dependency on well width.

EXPERIMENTAL METHODS

Chemicals and Materials. Organic halide salts were purchased from Greatcell Solar. All other chemicals were purchased from Sigma Aldrich.

Crystal and Film Synthesis. Perovskite single crystals were synthesized according to a previously reported slow-cooling precipitation method[26]. Briefly, lead oxide was dissolved in a heated solution of hydroiodic acid and hypophosphorous acid. The desired organic halide salts were added and dissolved. The solution was then allowed to cool, resulting in the precipitation of single crystal flakes. The flakes had lateral dimensions of up to several millimeters and micron-scale thicknesses. The crystals exhibit anisotropic growth because of the difference in bonding within the layers and between the layers. The crystals have larger dimensions in the plane of the quantum wells because the ionic bonds within the perovskite layers are stronger than the intermolecular forces between the layers. Thin films deposited by spin-casting and the antisolvent quenching method were

made following a previously reported procedure[19]. Briefly, a solution of precursor salts dissolved in γ-butyrolactone/dimethyl sulfoxide was deposited onto a glass substrate which was then spin-cast. The antisolvent chlorobenzene was dropped on the spinning film midway through the casting process. The films were then annealed. Perovskite nanoplatelets were synthesized according to a previously reported nonsolvent crystallization procedure[30] in which a solution of precursor salts in dimethylformamide was added drop-wise to an antisolvent vial of toluene. Films of perovskite nanoplatelets were deposited using a reported centrifugal casting method[29,30].

Materials Characterization. Film thickness measurements were done using an Asylum Research Cypher atomic force microscope (AFM). Films were scratched and imaged in tapping mode. Several measurements were made to determine the estimate of the global thickness.

Single Crystal Orientational Emission Measurement Single crystal flakes were exfoliated either by washing with hexane and dispersing on a glass coverslip (n = 1) or by using a polydimethylsiloxane (PDMS) stamp and pressing the crystals directly onto a glass coverslip (n = 2, 3). The orientational emission pattern for the single crystal flakes was

measured with a Fourier space microscopy setup. Samples were photoexcited with a 405 nm laser diode. An Olympus PlanApo N 60X Oil immersion objective (1.42NA) was used for pump injection and PL collection. The objective back focal plane was then imaged onto the entrance slit of a Princeton instruments IsoPlane 160 spectrometer with a liquid nitrogen cooled Princeton Instruments PyLoN 400BR camera. Light emitted from the edges of the crystals was blocked with a real-space filter. The pump intensity was attenuated to ensure the crystals were not being damaged. The PL wavelengths agreed with prior findings.[26]

Thin-film Orientational Emission Measurement. The orientational emission pattern for thin film samples was measured using a rotation mount. A 2 mW continuous wave laser source with a 405 nm wavelength served as the excitation source. The PL intensity was measured as a function of angle (-75 to 75 degrees, 1 degree increments) with a multimode fiber fixed on a rotation mount. PL was filtered using a 420 nm longpass filter and detected with an Ocean Optics spectrometer. Separate measurements were done for TE and TM polarizations. The TM datasets were rescaled such that the normal incidence PL intensity would match that of the corresponding TE datasets and care was

taken to minimize degradation during the measurement process. The datasets were then normalized to the TE PL maxima.

Dipole modelling. Modelling of the dipole emission within each material was done following the approach of Chance, Prock and Silbey.[27,28] Twenty layers of equidistant dipole emitter planes were used to model the films. The film thicknesses measured from AFM were used and the peak PL emission wavelengths were used. The films were fitted for the dipole orientation α, the in- and out-of-plane refractive indices, and a constant loss term κ to account for scattering and film inhomogeneity.

Density Functional Theory Calculations. DFT calculations were implemented through the CP2K software package[34] using a mixed Gaussian and plane-wave basis set. Pseudopotentials produced with the Goedecker-Teter-Hutter method[35] and were parameterized within the generalized gradient approximation with Perdew-Burke-Ernzerhof exchange-correlation functionals[36]. These were accompanied by the MOLOPT basis[37] and a 300 Ry grid charge density cutoff was used. Atomic positions and cell dimensions were simultaneously relaxed. Calculations were done for 18-cell supercells with in-plane dimensions of 25 Å and single layers of perovskite separated by 20 Å of

vacuum. The exciton was visualized by calculating the RMS expectation value of the separation between the LUMO and HOMO orbitals, $\sqrt{\langle\psi_2\psi_1|(r-r')^2|\psi_1\psi_2\rangle}$, on a 3D grid.[38] The software VESTA[39] was used for atomic illustration.

Polar Emission Patterns. The power radiated per solid angle for a perfect dipole follows,

$$\frac{dP}{d\Omega} \propto p_0^2 \sin^2 \alpha,$$

where p_0 is the dipole moment and α is the angle extending from the axis of the dipole to the point of interest. For an anisotropic emitter, the dipole moment can be represented as,

$$\frac{1}{p^2(\theta,\varphi)} = \frac{\cos^2\theta \sin^2\varphi}{p_x^2} + \frac{\sin^2\theta \sin^2\varphi}{p_y^2} + \frac{\cos^2\varphi}{p_z^2},$$

where p_x, p_y, and p_z are the cartesian components of the dipole moment and θ and φ are the polar and azimuthal angles. The power per solid angle for the anisotropic emitter is then,

$$\frac{dP}{d\Omega} \propto \int_0^{2\pi}\int_0^{\pi} p^2(\theta,\varphi) \sin^2(\alpha-\varphi) d\theta d\varphi.$$

Calculations for the power radiated as a function of α were done using the experimentally determined fractions of in-plane and out-of-plane transition dipole moment. The results were then normalized such that unit power was radiated.

LED Device Modelling. Optical simulations of LED emission efficiency were done through Finite-Differences Time-Domain numerical calculations implemented with the Lumerical FDTD Solutions software. The device was modelled as a thin film stack of layers: Al (100 nm, Lumerical built-in dispersion CRC), LiF (2 nm, optical properties from Li[40]), electron transport layer (50 nm, refractive index 1.75, transparent), perovskite (40 nm, experimentally determined optical properties from Proppe *et al.*[41]), hole transport layer (40 nm, refractive index 1.45, transparent), ITO (150 nm, optical properties from Walters *et al.*[29]), and glass (Lumerical built-in dispersion SiO_2 – Palik). A simulation volume of 4 × 4 × 1 microns with the long dimensions oriented in the plane of the device. Perfectly matched layer boundaries were used along with a non-uniform mesh. Light was injected into the system through radiative dipoles with emission spectra similar to the experimental ones and placed at the center of the perovskite film. Simulations were conducted for each case of the dipole oriented along the x, y, and z directions. The out-coupling efficiency for

a given case was determined by monitoring the power transmitted through the glass layer and normalized to the power output from the dipole. The EQE for the LED was calculated through an average of the powers transmitted, which were weighted according to the amount of dipole anisotropy. Unity photoluminescence quantum yield was assumed and electrical loss was excluded.

ASSOCIATED CONTENT

Supporting Information. Supporting Table S1 of the material emission wavelengths.

AUTHOR INFORMATION

Corresponding author

*Email: ted.sargent@utoronto.ca

ORCID

Grant Walters: 0000-0002-9005-2335

Louis Haeberlé: 0000-0002-1817-7985

Rafael Quintero-Bermudez: 0000-0002-4233-395X

Stéphane Kéna-Cohen: 0000-0001-5065-2750

Edward H. Sargent: 0000-0003-0396-6495

Author Contributions

§G.W. and L.H contributed equally to this work.

Notes

The authors declare no competing financial interest.

ACKNOWLEDGMENT

This publication is based on work supported by the United States Department of the Navy, Office of Naval Research (Grant Award No.: N00014-17-1-2524). S.K-C acknowledges support from the Canada Research Chairs program. G. W. acknowledges support from the Natural Sciences and Engineering Research Council of Canada (NSERC). G.W. and R.Q.B acknowledge invaluable help from Dr. Andrew Proppe.

REFERENCES

(1) Chiba, T.; Hayashi, Y.; Ebe, H.; Hoshi, K.; Sato, J.; Sato, S.; Pu, Y.-J.; Ohisa, S.; Kido, J. Anion-Exchange Red Perovskite Quantum Dots with Ammonium Iodine Salts for Highly Efficient Light-Emitting Devices. *Nat. Photonics* **2018**, *12* (11), 681–687.

(2) Xiao, Z.; Zhao, L.; Tran, N. L.; Lin, Y. L.; Silver, S. H.; Kerner, R. A.; Yao, N.; Kahn, A.; Scholes, G. D.; Rand, B. P. Mixed-Halide Perovskites with Stabilized Bandgaps. *Nano Lett.* **2017**, *17* (11), 6863–6869.

(3) Lin, K.; Xing, J.; Quan, L. N.; de Arquer, F. P. G.; Gong, X.; Lu, J.; Xie, L.; Zhao, W.; Zhang, D.; Yan, C.; Li, W.; Liu, X.; Lu, Y.; Kirman, J.; Sargent, E. H.; Xiong, Q.; Wei, Z. Perovskite Light-Emitting Diodes with External Quantum Efficiency Exceeding 20 per Cent. *Nature* **2018**, *562* (7726), 245–248.

(4) Zhang, L.; Yang, X.; Jiang, Q.; Wang, P.; Yin, Z.; Zhang, X.; Tan, H.; Yang, Y. (Michael); Wei, M.; Sutherland, B. R.; Sargent, E. H.; You, J. Ultra-Bright and Highly Efficient Inorganic Based Perovskite Light-Emitting Diodes. *Nat. Commun.* **2017**, *8*, 15640.

(5) Liu, Y.; Cui, J.; Du, K.; Tian, H.; He, Z.; Zhou, Q.; Yang, Z.; Deng, Y.; Chen, D.; Zuo, X.; Ren, Y.; Wang, L.; Zhu, H.; Zhao, B.; Di, D.; Wang, J.; Friend, R. H.; Jin, Y. Efficient Blue Light-Emitting Diodes Based on Quantum-Confined Bromide Perovskite Nanostructures. *Nat. Photonics* **2019**, *13* (11), 760–764.

(6) Li, Z.; Chen, Z.; Yang, Y.; Xue, Q.; Yip, H.-L.; Cao, Y. Modulation of Recombination Zone Position for Quasi-Two-Dimensional Blue Perovskite Light-Emitting Diodes with Efficiency Exceeding 5%. *Nat. Commun.* **2019**, *10*, 1027.

(7) Kim, J.-S.; Ho, P. K. H.; Greenham, N. C.; Friend, R. H. Electroluminescence Emission Pattern of Organic Light-Emitting Diodes: Implications for Device Efficiency Calculations. *J. Appl. Phys.* **2000**, *88* (2), 1073–1081.

(8) Schmidt, T. D.; Lampe, T.; Sylvinson M. R., D.; Djurovich, P. I.; Thompson, M. E.; Brütting, W. Emitter Orientation as a Key Parameter in Organic Light-Emitting Diodes. *Phys. Rev. Appl.* **2017**, *8*, 037001.

(9) Brütting, W.; Frischeisen, J.; Schmidt, T. D.; Scholz, B. J.; Mayr, C. Device Efficiency of Organic Light-Emitting Diodes: Progress by Improved Light Outcoupling. *Phys. Status Solidi A* **2013**, *210* (1), 44–65.

(10) Scott, R.; Heckmann, J.; Prudnikau, A. V.; Antanovich, A.; Mikhailov, A.; Owschimikow, N.; Artemyev, M.; Climente, J. I.; Woggon, U.; Grosse, N. B.; Achtstein, A. W. Directed Emission of CdSe Nanoplatelets Originating from Strongly Anisotropic 2D Electronic Structure. *Nat. Nanotechnol.* **2017**, *12* (12), 1155–1160.

(11) Gao, Y.; Weidman, M. C.; Tisdale, W. A. CdSe Nanoplatelet Films with Controlled Orientation of Their Transition Dipole Moment. *Nano Lett.* **2017**, *17* (6), 3837–3843.

(12) Jurow, M. J.; Lampe, T.; Penzo, E.; Kang, J.; Koc, M. A.; Zechel, T.; Nett, Z.; Brady, M.; Wang, L.-W.; Alivisatos, A. P.; Cabrini, S.; Brütting, W.; Liu, Y. Tunable Anisotropic Photon Emission from Self-Organized $CsPbBr_3$ Perovskite Nanocrystals. *Nano Lett.* **2017**, *17* (7), 4534–4540.

(13) Fieramosca, A.; De Marco, L.; Passoni, M.; Polimeno, L.; Rizzo, A.; Rosa, B. L. T.; Cruciani, G.; Dominici, L.; De Giorgi, M.; Gigli, G.; Andreani, L. C.; Gerace, D.; Ballarini, D.; Sanvitto, D. Tunable Out-of-Plane Excitons in 2D Single-Crystal Perovskites. *ACS Photonics* **2018**, *5* (10), 4179–4185.

(14) Zhang, Q.; Tavakoli, M. M.; Gu, L.; Zhang, D.; Tang, L.; Gao, Y.; Guo, J.; Lin, Y.; Leung, S.-F.; Poddar, S.; Fu, Y.; Fan, Z. Efficient Metal Halide Perovskite Light-Emitting Diodes with Significantly Improved Light Extraction on Nanophotonic Substrates. *Nat. Commun.* **2019**, *10*, 727.

(15) Zhao, L.; Lee, K. M.; Roh, K.; Khan, S. U. Z.; Rand, B. P. Improved Outcoupling Efficiency and Stability of Perovskite Light-Emitting Diodes Using Thin Emitting Layers. *Adv. Mater.* **2019**, *31* (2), 1805836.

(16) Jurow, M. J.; Morgenstern, T.; Eisler, C.; Kang, J.; Penzo, E.; Do, M.; Engelmayer, M.; Osowiecki, W. T.; Bekenstein, Y.; Tassone, C.; Wang, L.-W.; Alivisatos, A. P.; Brütting, W.; Liu, Y. Manipulating the Transition Dipole Moment of $CsPbBr_3$ Perovskite Nanocrystals for Superior Optical Properties. *Nano Lett.* **2019**, *19* (4), 2489–2496.

(17) Shen, Y.; Cheng, L.; Li, Y.; Li, W.; Chen, J.; Lee, S.; Tang, J. High-Efficiency Perovskite Light-Emitting Diodes with Synergetic Outcoupling Enhancement. *Adv. Mater.* **2019**, *31* (24), 1901517.

(18) Xiao, Z.; Kerner, R. A.; Zhao, L.; Tran, N. L.; Lee, K. M.; Koh, T.-W.; Scholes, G. D.; Rand, B. P. Efficient Perovskite Light-Emitting Diodes Featuring Nanometre-Sized Crystallites. *Nat. Photonics* **2017**, *11* (2), 108–115.

(19) Yuan, M.; Quan, L. N.; Comin, R.; Walters, G.; Sabatini, R.; Voznyy, O.; Hoogland, S.; Zhao, Y.; Beauregard, E. M.; Kanjanaboos, P.; Lu, Z.; Kim, D. H.; Sargent, E. H. Perovskite Energy Funnels for Efficient Light-Emitting Diodes. *Nat. Nanotechnol.* **2016**, *11* (10), 872–877.

(20) Wang, N.; Cheng, L.; Ge, R.; Zhang, S.; Miao, Y.; Zou, W.; Yi, C.; Sun, Y.; Cao, Y.; Yang, R.; Wei, Y.; Guo, Q.; Ke, Y.; Yu, M.; Jin, Y.; Liu, Y.; Ding, Q.; Di, D.; Yang, L.; Xing, G.; Tian, H.; Jin, C.; Gao, F.; Friend, R. H.; Wang, J.; Huang, W. Perovskite Light-Emitting Diodes Based on Solution-Processed Self-Organized Multiple Quantum Wells. *Nat. Photonics* **2016**, *10* (11), 699–704.

(21) Blancon, J.-C.; Stier, A. V.; Tsai, H.; Nie, W.; Stoumpos, C. C.; Traoré, B.; Pedesseau, L.; Kepenekian, M.; Katsutani, F.; Noe, G. T.; Kono, J.; Tretiak, S.; Crooker, S. A.; Katan, C.; Kanatzidis, M. G.; Crochet, J. J.; Even, J.; Mohite, A. D. Scaling Law for Excitons in 2D Perovskite Quantum Wells. *Nat. Commun.* **2018**, *9*, 2254.

(22) Tanaka, K.; Kondo, T. Bandgap and Exciton Binding Energies in Lead-Iodide-Based Natural Quantum-Well Crystals. *Sci. Technol. Adv. Mater.* **2003**, *4* (6), 599–604.

(23) Saidaminov, M. I.; Mohammed, O. F.; Bakr, O. M. Low-Dimensional-Networked Metal Halide Perovskites: The Next Big Thing. *ACS Energy Lett.* **2017**, *2* (4), 889–896.

(24) Quintero-Bermudez, R.; Gold-Parker, A.; Proppe, A. H.; Munir, R.; Yang, Z.; Kelley, S. O.; Amassian, A.; Toney, M. F.; Sargent, E. H. Compositional and Orientational Control in Metal Halide Perovskites of Reduced Dimensionality. *Nat. Mater.* **2018**, *17* (10), 900–907.

(25) Lin, Y.; Fang, Y.; Zhao, J.; Shao, Y.; Stuard, S. J.; Nahid, M. M.; Ade, H.; Wang, Q.; Shield, J. E.; Zhou, N.; Moran, A. M.; Huang, J. Unveiling the Operation Mechanism of Layered Perovskite Solar Cells. *Nat. Commun.* **2019**, *10*, 1008.

(26) Stoumpos, C. C.; Cao, D. H.; Clark, D. J.; Young, J.; Rondinelli, J. M.; Jang, J. I.; Hupp, J. T.; Kanatzidis, M. G. Ruddlesden-Popper Hybrid Lead Iodide Perovskite 2D Homologous Semiconductors. *Chem. Mater.* **2016**, *28*, 2852–2867.

(27) Chance, R.; Prock, A.; Silbey, R. *Molecular Fluorescence and Energy Transfer Near Interfaces*; Advances in Chemical Physics; John Wiley & Sons, 1978; Vol. 37.

(28) Moon, C.-K.; Kim, S.-Y.; Lee, J.-H.; Kim, J.-J. Luminescence from Oriented Emitting Dipoles in a Birefringent Medium. *Opt. Express* **2015**, *23* (7), A279.

(29) Walters, G.; Wei, M.; Voznyy, O.; Quintero-Bermudez, R.; Kiani, A.; Smilgies, D.-M.; Munir, R.; Amassian, A.; Hoogland, S.; Sargent, E. The Quantum-Confined Stark Effect in

Layered Hybrid Perovskites Mediated by Orientational Polarizability of Confined Dipoles. *Nat. Commun.* **2018**, *9*, 4214.

(30) Weidman, M. C.; Seitz, M.; Stranks, S. D.; Tisdale, W. A. Highly Tunable Colloidal Perovskite Nanoplatelets through Variable Cation, Metal, and Halide Composition. *ACS Nano* **2016**, *10* (8), 7830–7839.

(31) Even, J.; Pedesseau, L.; Katan, C.; Kepenekian, M.; Lauret, J.-S.; Sapori, D.; Deleporte, E. Solid-State Physics Perspective on Hybrid Perovskite Semiconductors. *J. Phys. Chem. C* **2015**, *119* (19), 10161–10177.

(32) Even, J.; Pedesseau, L.; Dupertuis, M.-A.; Jancu, J.-M.; Katan, C. Electronic Model for Self-Assembled Hybrid Organic/Perovskite Semiconductors: Reverse Band Edge Electronic States Ordering and Spin-Orbit Coupling. *Phys. Rev. B* **2012**, *86* (20), 205301.

(33) Proppe, A. H.; Quintero-Bermudez, R.; Tan, H.; Voznyy, O.; Kelley, S. O.; Sargent, E. H. Synthetic Control over Quantum Well Width Distribution and Carrier Migration in Low-Dimensional Perovskite Photovoltaics. *J. Am. Chem. Soc.* **2018**, *140* (8), 2890–2896.

(34) VandeVondele, J.; Krack, M.; Mohamed, F.; Parrinello, M.; Chassaing, T.; Hutter, J. Quickstep: Fast and Accurate Density Functional Calculations Using a Mixed Gaussian and Plane Waves Approach. *Comput. Phys. Commun.* **2005**, *167* (2), 103–128.

(35) Hartwigsen, C.; Gø edecker, S.; Hutter, J. Relativistic Separable Dual-Space Gaussian Pseudopotentials from H to Rn. *Phys. Rev. B* **1998**, *58* (7), 3641–3662.

(36) Perdew, J. P.; Burke, K.; Ernzerhof, M. Generalized Gradient Approximation Made Simple. *Phys. Rev. Lett.* **1996**, *77* (18), 3865–3868.

(37) VandeVondele, J.; Hutter, J. Gaussian Basis Sets for Accurate Calculations on Molecular Systems in Gas and Condensed Phases. *J. Chem. Phys.* **2007**, *127* (11),

(38) Arora, A.; Drüppel, M.; Schmidt, R.; Deilmann, T.; Schneider, R.; Molas, M. R.; Marauhn, P.; Michaelis de Vasconcellos, S.; Potemski, M.; Rohlfing, M.; Bratschitsch, R. Interlayer Excitons in a Bulk van Der Waals Semiconductor. *Nat. Commun.* **2017**, *8* (1), 639.

(39) Momma, K.; Izumi, F. *VESTA 3* for Three-Dimensional Visualization of Crystal, Volumetric and Morphology Data. *J. Appl. Crystallogr.* **2011**, *44* (6), 1272–1276.

(40) Li, H. H. Refractive Index of Alkali Halides and Its Wavelength and Temperature Derivatives. *J. Phys. Chem. Ref. Data* **1976**, *5* (2), 329–528.

(41) Proppe, A. H.; Walters, G. W.; Alsalloum, A. Y.; Zhumekenov, A. A.; Mosconi, E.; Kelley, S. O.; De Angelis, F.; Adamska, L.; Umari, P.; Bakr, O. M.; Sargent, E. H. Transition Dipole Moments of n = 1, 2, and 3 Perovskite Quantum Wells from the Optical Stark Effect and Many-Body Perturbation Theory. *J. Phys. Chem. Lett.* **2020**, *11* (3), 716–723.